Check for updates

Visible-light-driven photo-peroxidase catalysis: high-efficiency degradation of indole in water

Chongrui Xu, Ping Xue, [ID] * Rui Li, Juan Jia, Linmeng Ma and Peng Li

The demand for H_2O_2 restricts the wider application of horseradish peroxidase (HRP) in degradation. In this work, a novel photoenzyme synergistic catalytic system was developed for high-efficiency degrading of indole in water by HRP without extra H_2O_2. The HRP was immobilized on CN-ZIF prepared by the combination of g-C_3N_4 and ZIF-8 to achieve photo-peroxidase catalyst HRP/Zn-CN-ZIF. Under visible light, photogenerated electrons and H_2O_2 from HRP/Zn-CN-ZIF participated in the biocatalytic cycle of HRP directly. As a result, the indole at 20 mg L^{-1} in water was degraded completely in 2 h by the HRP/Zn-CN-ZIF photoenzyme synergistic catalytic system without the addition of H_2O_2. Furthermore, HRP/Zn-CN-ZIF exhibited superior visible light absorption and charge transfer ability compared to g-C_3N_4. The results of the mechanism studies suggest that ·OH would play the most significant role from the HRP/Zn-CN-ZIF in indole degradation. This research provides an efficient approach for the removal of indole from water environments.

1. Introduction

The water pollution originating from industrial activities poses a critical threat to the survival of hydrobios and humans. As a common nitrogen-containing heterocyclic compound, indole has been extensively utilized in medicine manufacture. The petrochemical industry and intensive livestock production have contributed to significant emissions of indole.[1,2] Indole has the potential to induce hemoglobinuric nephrosis, temporary skin irritation, and tumor formation.[3] Given these challenges, it is crucial and urgent to explore effective solutions for the removal of indole from wastewater in order to mitigate its harmful consequences.

At present, the available methods for indole elimination primarily include chemical removal,[4,5] physical adsorption,[6,7] and biological degradation.[8,9] In recent years, enzymatic degradation as a biological treatment method has gained increasing popularity, owing to its numerous advantages, including environmental friendliness, efficient removal performance, and the capacity to eliminate a variety of pollutants.[10] As a typical oxidoreductase, horseradish peroxidase (HRP, EC 1.11.1.7) has garnered significant attention for its extensive utilization in biocatalytic degradation of diverse refractory organics, and demonstrated exceptional potential in water treatment.[11–13] However, according to relevant reports, the degradation effect of HRP on indole is limited without redox mediators.[11,14] Unfortunately, the addition of mediators not

State Key Laboratory of High-efficiency Coal Utilization and Green Chemical Engineering, College of Chemistry & Chemical Engineering, Ningxia University, Yinchuan 750021, China. E-mail: ping@nxu.edu.cn

only increases costs, but may also cause secondary pollution. Furthermore, HRP can only participate in redox reactions in the company of H_2O_2, thereby achieving the removal of organic contaminants. As is well known, H_2O_2, as a strong oxidant, may cause explosions during its manufacturing and use, and its safety risks and additional costs limit the application of HRP.

To overcome the limitations of HRP, the combination of enzyme catalysis and photocatalysis has been recognized as an effective strategy.[15,16] Because solar energy can be directly used to drive the reaction, photocatalysis has become a widely concerned method for removing organic pollutants in water. Jiang[17] *et al.* prepared MoS_2/CN-PEI photocatalysts with the assistance of surfactant PEI and used this catalyst to degrade rhodamine B. The flower-sphere-like structure of MoS_2/CN-PEI shortens the transport distance of charge carriers and promotes their transfer in heterojunctions, thereby achieving complete substrate degradation. Chen[18] *et al.* prepared $Zn_3In_2S_6$ photocatalyst with S defects, which was used to degrade three different antibiotics. The results showed that the introduction of S defects improved the carrier mobility of the catalyst, thereby enhancing its degradation performance for antibiotics. It is essential to emphasize that photocatalysts for enzyme immobilization need to meet a series of criteria, including excellent photocatalytic activity, chemical stability, biocompatibility, and low toxicity.[19] Among the various materials used for photocatalysis, graphitic carbon nitride (g-C_3N_4) has garnered extensive attention on account of its low cost and visible light response.[20] As a non-metallic semiconductor composed solely of carbon and nitrogen element, g-C_3N_4 has a band gap of about 2.7 eV.[21] This non-metallic material exhibits excellent stability and resistance to acids, alkalis, and photo-corrosion.[22]

Moreover, g-C_3N_4 exhibits remarkable degradation activity towards a diverse set of organic pollutants in water, including dye and phenol,[23] and showcases favorable biocompatibility,[15,24] making it a suitable carrier for enzyme immobilization. What is more important, g-C_3N_4 has the capability to generate the required H_2O_2 for the redox cycle of HRP under visible light irradiation during the photoenzyme synergistic degradation reaction.[15,25,26]

Herein, a novel photo-peroxidase catalyst was prepared by the combination of ZIF-8 and g-C_3N_4 and the immobilization of HRP. The introduction of ZIF-8 improved the light absorption ability and carrier mobility of the catalyst. During the degradation process, not only the photocatalyst participated in the degradation, but HRP could also significantly improve the reaction efficiency by utilizing H_2O_2 under visible light irradiation, ultimately achieving complete degradation of indole. In addition, the indole degradation ability of the photo-peroxidase catalyst did not decrease significantly after 4 cycles. Finally, the possible mechanism of the photoenzyme synergistic catalytic is discussed. The photo-peroxidase catalytic provides a feasible thought for the treatment of indole in the practical industrial application.

2. Experimental

2.1. Materials

Horseradish peroxidase (HRP, $\geq$150 U mg^{-1}) was provided from TCI (Shanghai). Urea (AR, $\geq$99%), $Zn(NO_3)_2 \cdot 6H_2O$ (AR, $\geq$99%), EDTA-2Na (AR, $\geq$99%), and H_2O_2 (AR, $\geq$30%) were obtained from Sinopharm Chemical Reagent. Indole (99%), $Zn(OAc)_2$ (99.5%), brilliant blue G-250 (AR), and 1,4-benzoquinone (PBQ, 99%) were obtained from Beijing InnoChem Science & Technology. 2-Methylimidazole (98%) was provided from Shanghai Aladdin Biochemical Technology. 4-Aminoantipyrine (99%) was provided from Shanghai Adamas Reagent. Isopropanol (IPA, AR, $\geq$99.7%) was provided from Xilong Scientific.

2.2. Preparation of the photo-peroxidase catalyst

In a muffle furnace, a covered 10 mL alumina crucible containing about 6 g of urea was calcined at 550 °C for 180 min. The heating rate was 10 °C min^{-1}. In order to obtain g-C_3N_4, the solid formed in the crucible was cooled and ground. 28.5 mL of methanol was respectively used to dissolve zinc nitrate hexahydrate (0.6 g) and 2-methylimidazole (1.32 g). The 2-methylimidazole solution was mixed with the zinc nitrate hexahydrate solution gradually and stirred for 60 min. After centrifuging the resulting mixture, ZIF-8 was obtained by rinsing with methanol and drying at 60 °C overnight. Equal masses of g-C_3N_4 and ZIF-8 were added to 20 mL of deionized water and stirred for 3 h. The resulting precipitate was dried overnight to obtain the precursor after centrifuging the mixture at 8000 rpm for 5 min. The precursor was placed in a tube furnace and calcined at 400 °C for 2 h in nitrogen. The heating rate was 5 °C min^{-1}. The solid was obtained after cooling and named CN-ZIF.

Subsequently, 50 mg of CN-ZIF was dispersed in 20 mL of deionized water. Then, 10 mg of $Zn(OAc)_2$ was mixed with the CN-ZIF dispersion and stirred for 3 h. A certain amount of HRP was mixed with the suspension gradually. Then, the suspension was oscillated at 150 rpm and 25 °C for 2 h in a constant temperature oscillator. During this process, the carrier and enzyme were connected through zinc coordination. The photo-peroxidase catalyst was obtained after centrifugation and named HRP/Zn-CN-ZIF.

2.3. Characterizations

In this work, an X-ray diffractometer (D8 ADVANCE A25, Bruker) was used to perform the X-ray diffraction (XRD) analysis. Fourier transform infrared (FTIR) was measured on a Perki-nElmer Spectrum Two FTIR spectrometer with KBr tablet technology. A field-emission scanning electron microscope (FESEM, Regulus8100, Hitachi) with energy dispersive X-ray technology was used to acquire the images of SEM. The measurements of X-ray photoelectron spectroscopy (XPS) were performed using an X-ray photoelectron spectrometer (AXIS SUPRA+, Shimadzu). A spectrophotometer (U-4100, Hitachi) was used to measure UV-visible diffuse reflectance spectra (UV-vis DRS) at 200–800 nm wavelength range. Total organic carbons (TOC) were measured by a TAILIN HTY-CT1000B analyzer. The electron paramagnetic resonance (EPR) analyses were carried out by a JEOL JES-FA200 electron spin resonance spectrometry. The electrochemical impedance spectra (EIS), transient photocurrent, and Mott–Schottky curve of the samples were acquired via a Model CHI 760E workstation (CH Instruments) in 0.5 M Na_2SO_4 solution.

2.4. Degradation of indole

In the degradation reaction, a 300 W xenon lamp (MC-PF300, Beijing MerryChange) with an optical filter (>420 nm) was employed to provide the visible light. 50 mg of catalyst was added to the 50 mL indole solution (20 mg L^{-1}) at room temperature. The mixture was stirred in darkness for 1 h to avoid the impact of adsorption on measurement results. Subsequently, the light irradiation was initiated. 0.5 mL of supernatant in the reactor was collected at regular intervals for the determination of indole concentration. A high-performance liquid chromatography workstation (HPLC, Agilent 1260 Infinity II) with a UV/visible detector was used to measure the concentration of indole. The measurement was performed on a C18 analytical column (5 μm), and the mobile-phase was made up of methanol and deionized water (80 : 20 v/v). The detection wavelength was 254 nm, and the column temperature was 30 °C. In the cyclic test, the catalyst is isolated through centrifugation at 8000 rpm and rinsed with deionized water, and reused under the same conditions.

2.5. Activity assay of the photo-peroxidase catalyst

The activity of HRP was measured by the colorimetric assay.[27] 1.62 g of phenol was dissolved in 100 mL of deionized water, and then add 0.05 g of 4-aminoantipine to obtain the 4-aminoantipine solution. 1.5 mL of this solution and 1.5 mL of H_2O_2 solution diluted with phosphate buffer (pH 7.0) to 0.006% was add to a quartz cuvette. Then, 1 mg of HRP/Zn-CN-ZIF sample

was added. A UV-visible spectrophotometer was used to measure the absorbance of red color product at 510 nm at regular intervals. The activity of photo-peroxidase catalyst can be determined using the following formula: (1)

$$\text{Enzyme activity}\left(\text{U mg}^{-1}\right) = \frac{E_{510} \times V}{\Delta A \times E_w} \qquad (1)$$

where E_{510} represents the rate of absorbance increase per minute at 510 nm; V denotes the total volume of the reaction solution; ΔA signifies that 1 unit of HRP causes an absorbance increase of 6.58 per minute; and E_w corresponds to the mass of the immobilized enzyme in the mixture. For the above cases, 1 unit of the activity (U) represented the amount of HRP that was required to consume 1 μmol of H_2O_2 per minute.

2.6. Enzyme loading measurement

The enzyme loading of HRP/Zn-CN-ZIF was determined by the Bradford method.[28] The initial enzyme solution and the supernatant after immobilization were added to Coomassie brilliant blue G-250 solution, respectively. After reaction for 3 min, a UV-visible spectrophotometer was used for determining the absorbance at 595 nm. There is a direct proportion between the absorbance and the concentration of protein in the solution. Specifically, the loading amount of HRP can be determined using the following formula: (2)

$$\text{Loading amount}\left(\text{mg g}^{-1}\right) = \frac{(C_0 - C)V}{m} \qquad (2)$$

where m is the mass of the carrier; C_0 and C are the concentration of initial enzyme solution and the concentration of enzyme in the supernatant; V represents the volume of the enzyme solution and supernatant.

3.   Results and discussion

3.1.   Characterizations of the catalysts

The XRD patterns of HRP/Zn-CN-ZIF, CN-ZIF, g-C₃N₄ and ZIF-8 are displayed in Fig. 1a. The characteristic diffraction peaks of

ZIF-8 and g-C₃N₄ appear simultaneously in the pattern of CN-ZIF, indicating that these two materials have been combined successfully. Specifically, for g-C₃N₄ at 13.0°, the diffraction peak can be ascribed to the (100) crystal planes of triazine units; the diffraction peak at 27.4° can be ascribed to the (002) crystal planes, which represents the interlayer stacking of the aromatic systems.[29] In addition, the diffraction peaks at 7.3°, 10.3°, 12.7°, 16.5°, and 18.0° belong to the (011), (002), (112), (013), and (222) crystal planes of ZIF-8, respectively.[30] The patterns of HRP/Zn-CN-ZIF and CN-ZIF are similar, indicating that the crystal structure of the catalyst remains essentially unchanged after immobilizing HRP. Fig. 1b shows the spectra of FTIR within the extent of 4000–400 cm⁻¹. In the spectrum of HRP/Zn-CN-ZIF, the peak at 2965 cm⁻¹ corresponds to –CH₂/–CH₃, indicating the successful immobilization of HRP.[15] For CN-ZIF, the spectrum displays the characteristic absorption peaks of both g-C₃N₄ and ZIF-8, which is similar to the results of XRD. The absorption peaks which appeared between 3000 cm⁻¹ and 3500 cm⁻¹ are corresponded to the N–H stretching vibrations of the amino and imino groups in CN-ZIF and g-C₃N₄. The absorption peaks at 807 cm⁻¹ and 1200–1650 cm⁻¹ of CN-ZIF and g-C₃N₄ belong to the breathing mode and stretching mode of the triazine units.[22] It has been shown that for CN-ZIF and ZIF-8, at 990 cm⁻¹ and 1145 cm⁻¹, the absorption peaks originate from the stretching vibrations of the C–N bonds in the imidazole structure, while the peak at 422 cm⁻¹ is related to the stretching vibrations of the Zn–N bonds.[31] Furthermore, the characteristic absorption peaks observed at 2933 cm⁻¹ and 3138 cm⁻¹ can be ascribed to the stretching vibrations of the C–H bonds in the imidazole rings and methyl of ZIF-8, respectively.[31] XRD and FTIR were characterized for HRP/Zn-CN-ZIF after 2 h of reaction. The XRD pattern and FTIR spectrum of used HRP/Zn-CN-ZIF suggest no significant changes, indicating the good stability of the catalyst.

The measurements of images SEM were conducted to study the morphologies of the catalysts. As shown in Fig. 2c, HRP/Zn-CN-ZIF is composed of the irregular sheet-like structure, which is basically consistent with g-C₃N₄ (Fig. 2a). It was found from

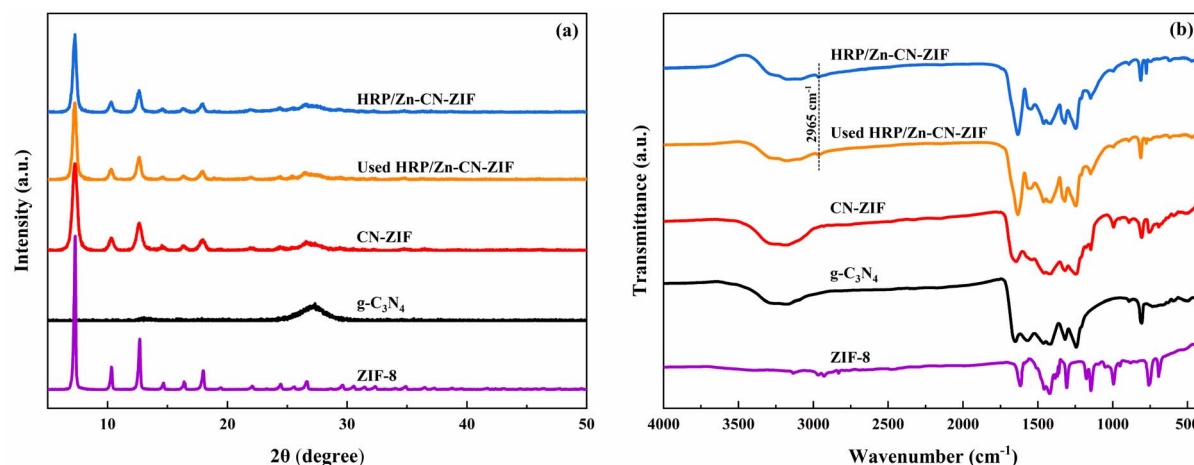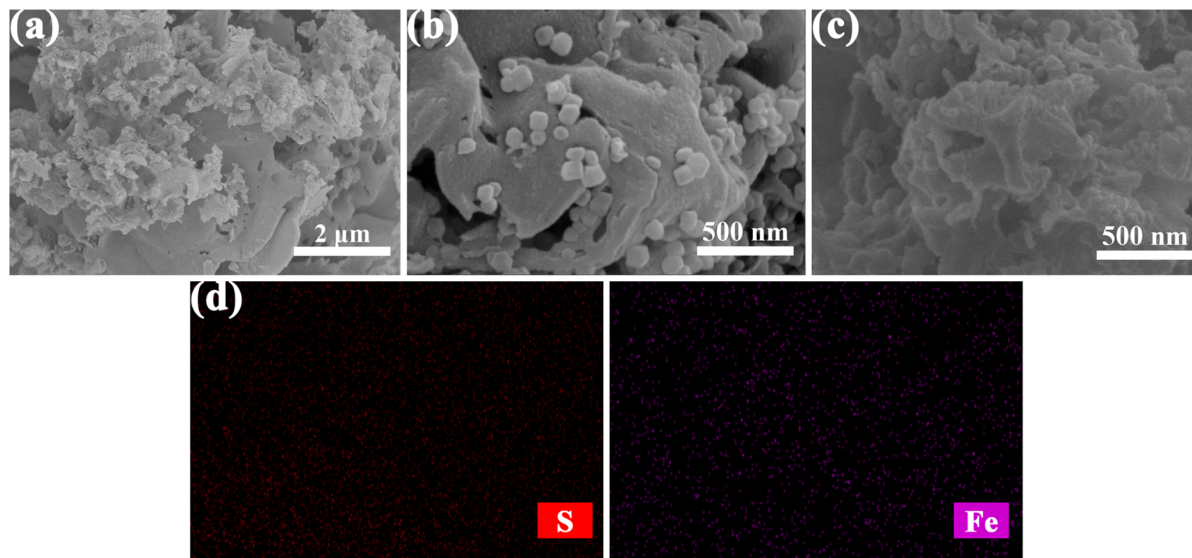**Fig. 1** XRD patterns (a) and FTIR spectra (b) of HRP/Zn-CN-ZIF, CN-ZIF, g-C₃N₄ and ZIF-8.

Fig. 2 SEM images of g-C$_3$N$_4$ (a), CN-ZIF (b), HRP/Zn-CN-ZIF (c), and EDS-mapping of HRP/Zn-CN-ZIF (d).

Fig. 2b and c that some granular structures appear on the surface of CN-ZIF and HRP/Zn-CN-ZIF, which proves that ZIF-8 has successfully loaded onto the surface of g-C$_3$N$_4$. Neither the loading of ZIF-8 nor the immobilization of HRP significantly altered the morphology of g-C$_3$N$_4$. In addition, the S and Fe element in EDS-mapping further proves the immobilization of HRP.

The chemical states of the composites were studied by XPS. Fig. 3a shows the C 1s spectrum, where the peaks at 288.0, 258.7, and 284.8 eV are ascribed to N–C=N, C–N, and C–C

bonds, respectively.[31] Fig. 3b displays three peaks at 400.9, 399.5, and 398.3 eV, ascribing to graphitic N, pyrrolic N, and sp^2 pyridinic N.[32] According to the spectra, the proportion of pyridine N in the catalyst is relatively high, which is conducive to promoting charge transfer due to the lower electron transfer barrier of pyridine N.[33] The peaks at 1045.2 and 1022.2 eV in Fig. 3c correspond to Zn 2p$_{1/2}$ and Zn 2p$_{3/2}$.[30] It should be pointed out that after the immobilization of HRP, some binding energy peaks exhibit slight shifts compared to their positions on the CN-ZIF sample, which can be associated with the strong
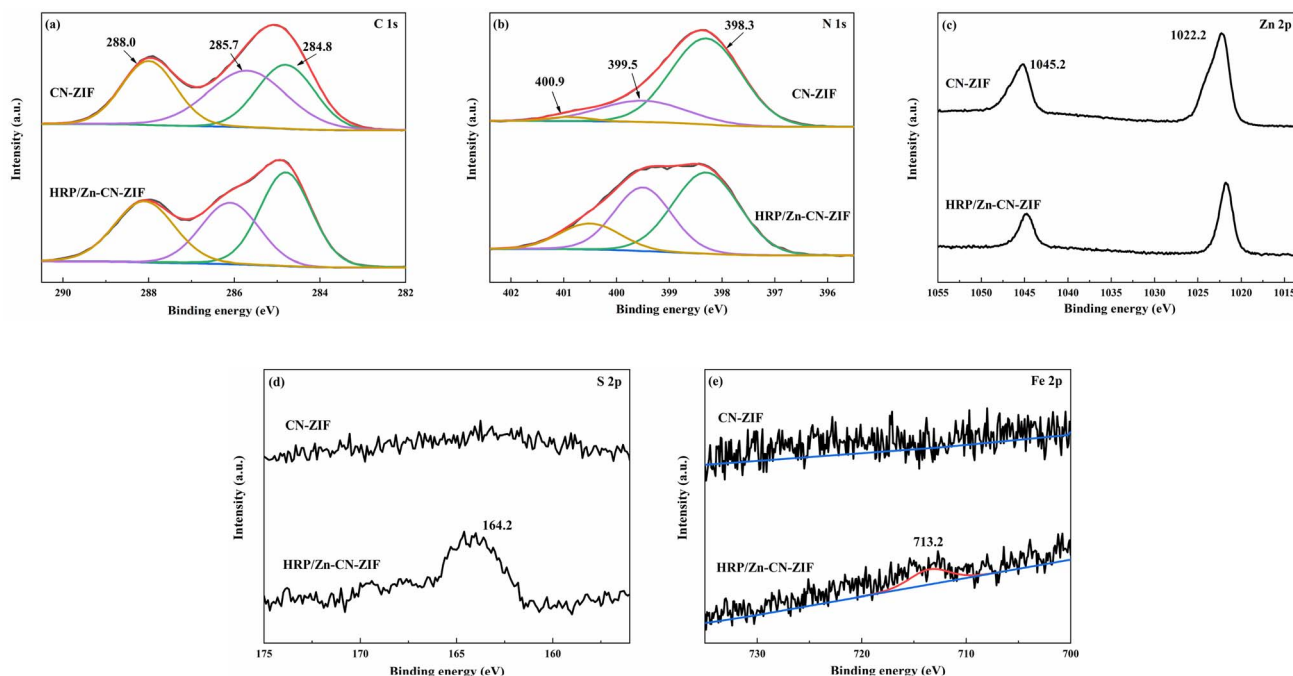

Fig. 3 XPS spectra of CN-ZIF and HRP/Zn-CN-ZIF: C 1s (a), N 1s (b), Zn 2p (c), S 2p (d) and Fe 2p (e).

interaction between HRP and CN-ZIF. In addition, the peak of S 2p at 164.2 eV (Fig. 3d) and the weak peak of Fe 2p at 713.2 eV (Fig. 3e) further demonstrate the immobilization of HRP on CN-ZIF.[15,19]

The UV-vis DRS pattern was measured to evaluate the light-absorbing capacity of the catalyst, as shown in Fig. 4a. By comparison to g-C_3N_4, CN-ZIF clearly exhibits enhanced light absorption ability in the region of visible light after compounding with ZIF-8, which significantly improves its utilization efficiency of solar energy. This phenomenon may be attributed to the carbonization of ZIF-8 and the covalent bonds between g-C_3N_4 and ZIF-8.[26] Moreover, as shown in Fig. 4b, the approximate calculation of band gap energy (E_g) for the photocatalyst was according to the Tauc equation:[34,35] eqn (3).

$$(\alpha h\nu)^{1/2} = C(h\nu - E_g) \tag{3}$$

where α represents absorption coefficient, h is the Planck constant, ν denotes frequency, and C is a constant. It is worth noting that after immobilizing HRP, the band gap of CN-ZIF decreases from 2.09 eV to 2.04 eV. This reduction facilitates the easier excitation of electrons from the valence band to the conduction band, thereby further enhancing its photocatalytic performance.[36]

The measurements of electrochemical impedance were utilized to assess the capability of charge separation and transfer of the catalysts. Fig. 5a shows the results achieved. Comparing to CN-ZIF and g-C_3N_4, the Nyquist curve radius of HRP/Zn-CN-ZIF is smaller, which means HRP/Zn-CN-ZIF possesses lower interfacial resistance and stronger electron transfer performance. This favors the enhancement of photocatalytic performance.[37] Moreover, as shown in Fig. 5b, g-C_3N_4 exhibits the lowest photocurrent density. After compounding with ZIF-8, the photocurrent density of the composite material significantly increases. Furthermore, HRP/Zn-CN-ZIF demonstrates higher photocurrent density compared to CN-ZIF. This indicates that after immobilizing HRP, the interfacial photogenerated charge separation efficiency and carrier mobility of the catalyst are improved, which further enhances the catalytic

efficiency.[38] The Mott–Schottky plots are shown in Fig. 5c. The curves in the graph all exhibit positive slopes, indicating that these samples belong to n-type semiconductors. The flat band potentials of g-C_3N_4, CN-ZIF, and HRP/Zn-CN-ZIF are −1.12 V, −1.41 V, and −1.37 V (vs. Ag/AgCl) or −0.92 V, −1.21 V, and −1.17 V (vs. NHE),[39] respectively. In the case of n-type semiconductor, the bottom of the conduction band (E_{CB}) almost has the same value with the flat band potential. Through the equation $E_g = E_{VB} - E_{CB}$ and the previously obtained E_g, we can deduce that the valence band (VB) positions of these three catalysts are 1.71 eV, 0.68 eV, and 0.67 eV (vs. NHE), respectively.

3.2. Degradation of indole

The degradation performance of the catalyst was assessed by conducting removal experiments of indole. The degradation curves of different catalysts towards indole are shown in Fig. 6a. Within two hours, HRP/Zn-CN-ZIF achieved complete degradation of indole. However, under the same conditions, g-C_3N_4 and CN-ZIF only exhibited degradation rates of 50.5% and 79.0%, respectively. In addition, the degradation rate constants were fitted by the pseudo-first-order kinetic equation. Based on the plots of $\ln(C/C_0)$ versus time displayed in Fig. 6b, the degradation rate constant for indole by HRP/Zn-CN-ZIF is 0.04169 min^{-1}, significantly higher than that of g-C_3N_4 (0.00542 min^{-1}) and CN-ZIF (0.01275 min^{-1}). Furthermore, as shown in Fig. 6c, compared to the TOC removal rate of g-C_3N_4 (19.37%) and CN-ZIF (27.13%), the rate of HRP/Zn-CN-ZIF is higher, and it reaches 41.28% after 2 h of reaction. The above results indicate that in comparison with the other two catalysts, HRP/Zn-CN-ZIF has stronger degradation performance for indole. The cyclic stability of HRP/Zn-CN-ZIF was evaluated, and the result is indicated in Fig. 6d. After four cycles, it is evident that although the degradation rate has reduced, the HRP/Zn-CN-ZIF can still maintain a high degradation rate for indole. The above results indicate that the prepared HRP/Zn-CN-ZIF has good reusability in indole degradation and can effectively maintain enzyme activity, thereby achieving stable and continuous degradation of indole.
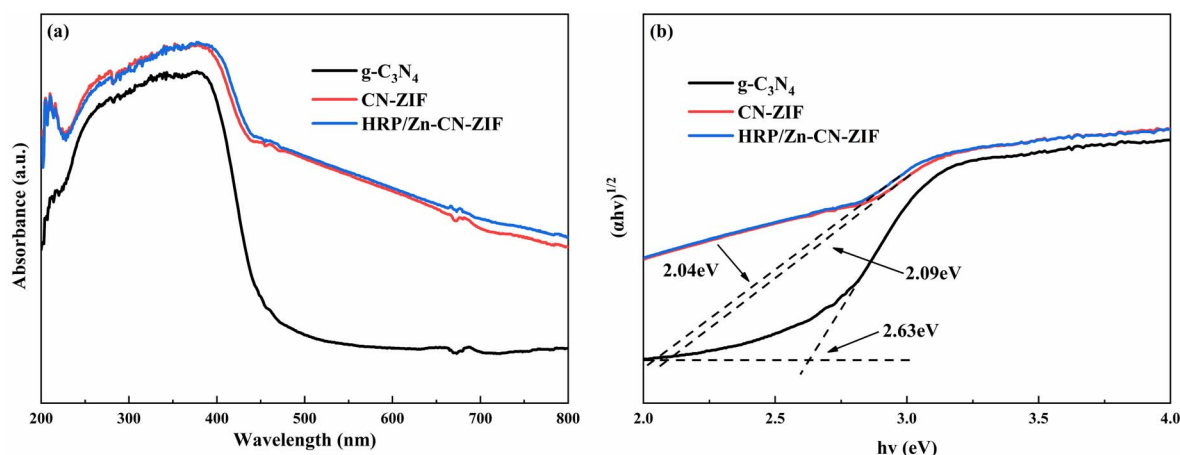

Fig. 4 UV-vis DRS (a) and plots of $(\alpha h\nu)^{1/2}$ versus $h\nu$ (b) for HRP/Zn-CN-ZIF, CN-ZIF and g-C_3N_4.
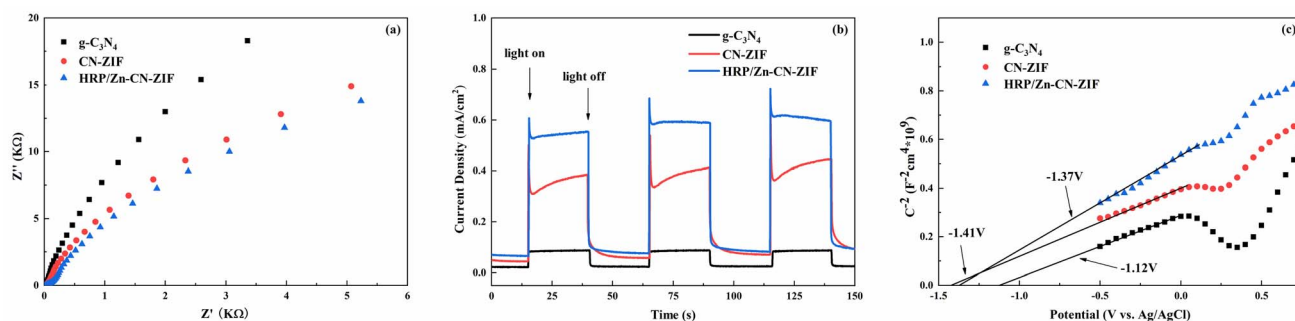
Fig. 5 EIS Nyquist plots (a), transient photocurrent responses (b), and Mott–Schottky curves (c) of HRP/Zn-CN-ZIF, CN-ZIF and g-C_3N_4.

The influence of different dosages of enzyme during the enzyme immobilization on degradation was investigated. Fig. 7a shows that the catalyst displayed the highest degradation rate of indole when the concentration of enzyme in the immobilization process was 1 mg mL^{-1}. When the concentration of HRP decreased to 0.75 and 0.5 mg mL^{-1}, a certain decline in degradation rate was observed. However, when the enzyme concentration further dropped to 0.25 mg mL^{-1}, a more

pronounced decrease in degradation rate occurred, and complete degradation of the substrate within 2 h was not achieved. The enzyme loading amount on CN-ZIF and the activity of immobilized enzyme under different dosages of HRP are shown in Table 1. When the concentration of HRP was 1 mg mL^{-1} during the process of enzyme immobilization, the HRP loading amount could reach 149.2 mg g^{-1}. As the enzyme concentration decreased during the immobilization process, the HRP loading
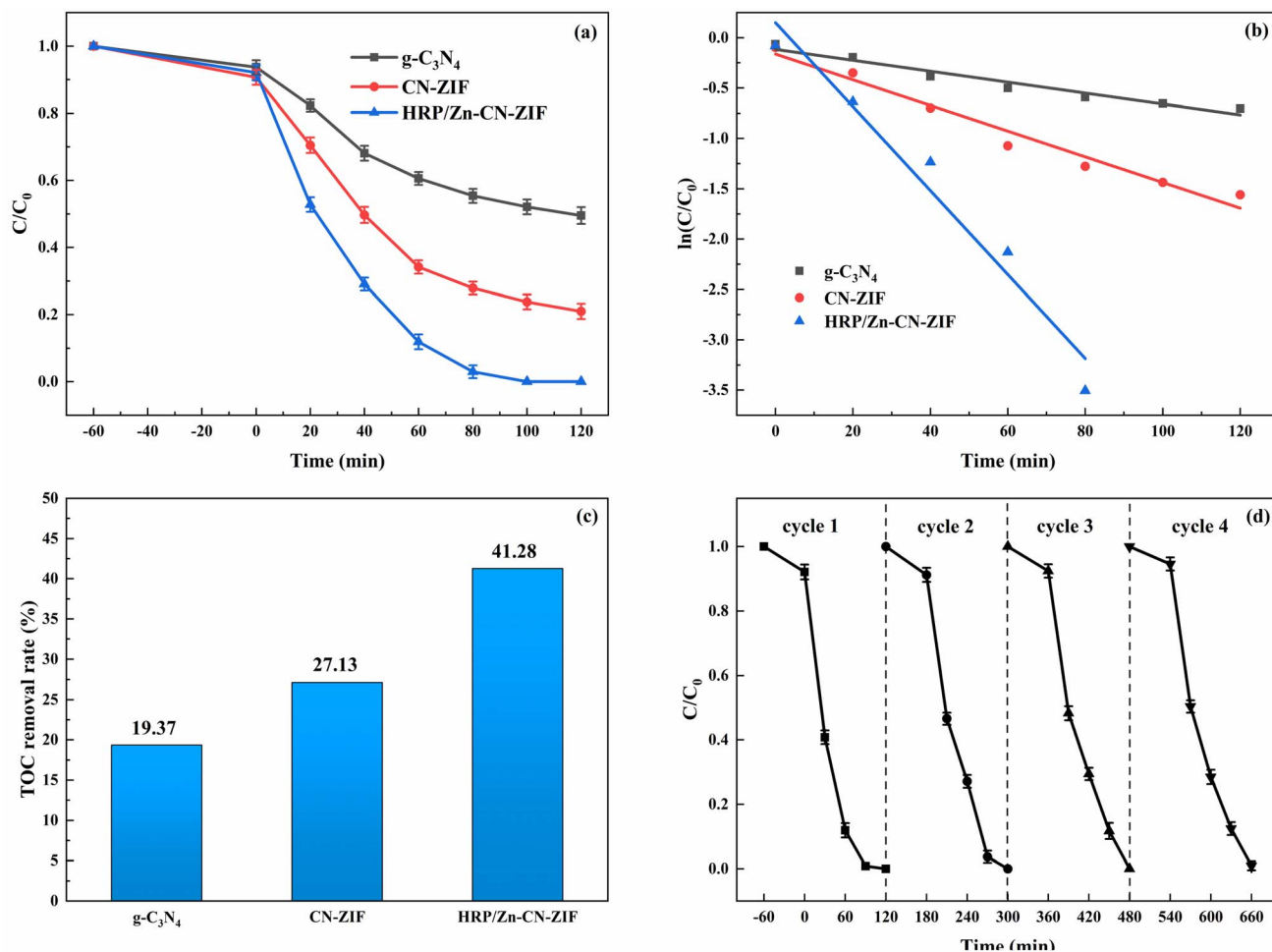

Fig. 6 Degradation (a), plots of ln(C/C_0) versus time (b), and TOC removal rates (c) of indole by using different catalysts, cycle degradation curves of indole by HRP/Zn-CN-ZIF (d).
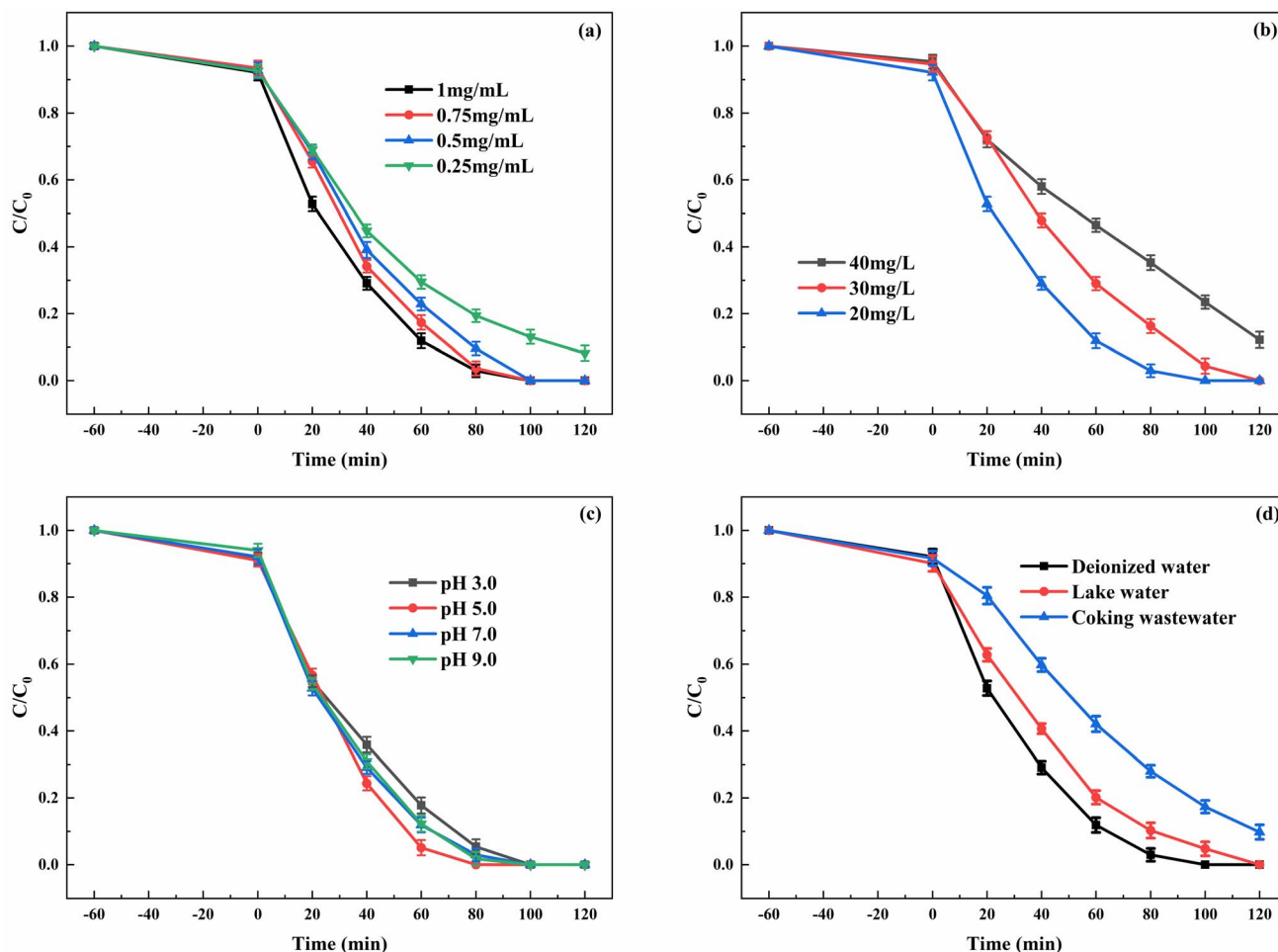
Fig. 7 Indole degradation by HRP/Zn–CN–ZIF at different dosages of HRP (a), substrate concentrations (b), different pH (c), and in different water bodies (d), the concentration of indole was 20 mg L^{-1} in (a), (c), and (d).

Table 1 Effect of the HRP dosages on the loading amount and the activity of immobilized enzyme

Concentration of HRP (mg mL^{-1})	Enzyme loading (mg g^{-1})	Enzyme activity (U mg^{-1})
0.25	46.8	5.1
0.5	104.0	10.9
0.75	133.6	14.2
1.0	149.2	16.6

amount and the activity of immobilized enzyme also decreased accordingly. Especially, when the enzyme concentration dropped to 0.25 mg mL^{-1}, the HRP loading amount significantly decreased to 46.8 mg g^{-1}, leading to the decline in the reaction rate during the degradation process. Fig. 7b shows the effect of indole concentration in the photo-peroxidase synergistic degradation. Although in the 40 mg L^{-1} indole solution, the degradation rate of substrate by HRP/Zn–CN–ZIF still reached 87.8% after 2 h of reaction. This result proves that the photo-peroxidase catalyst can maintain good degradation performance at high substrate concentrations. It is well known that

pH has a critical influence on enzyme activity. Both excessively high and low pH values can cause changes in the protein conformation, leading to the inactivation of enzymes. The degradation of indole by HRP/Zn–CN–ZIF under various pH values was studied, as shown in Fig. 7c. When the pH decreased from 7.0 to 5.0, the reaction rate showed a slight increase, attributed to the maximum activity of HRP in the mildly acidic environment.[40] Furthermore, there was a slight decrease in degradation rate at pH 3.0 and 9.0. Overall, the HRP/Zn–CN–ZIF exhibited excellent degradation activity when the pH was in the range of 3.0 to 9.0. In order to study the degradation performance of the catalyst in actual water bodies, the degradation of indole was carried out in deionized water, lake water, and coking wastewater, and the results are shown in Fig. 7d. The lake water was collected from Ningda Lake, and the coking wastewater was obtained from Ningdong Energy Chemical Industry Base in Ningxia. Lake water and coking wastewater had undergone preliminary physical treatment before the experiment. The degradation efficiency of indole was decreased in the lake water and coking wastewater due to the more complex composition. In particular, the degradation rate was 90.2% in the coking wastewater. This may be due to the influence of

enzyme activity and the competition of organic pollutants and inorganic ions for the reactive species. In general, HRP/Zn-CN-ZIF showed good degradation performance in different water bodies.

To discuss the influence of different radicals in the process of photoenzyme degradation, PBQ (1 mM) was used as the free radical scavenger in the system to remove superoxide radicals ($\cdot O_2^-$). Similarly, hydroxyl radicals ($\cdot OH$) and photogenerated holes (h^+) were removed by IPA (10 mM) and EDTA-2Na (10 mM). As shown in Fig. 8a, upon the addition of PBQ, IPA, and EDTA-2Na, the corresponding indole degradation rates after 2 h of reaction decrease to 65.03%, 33.17%, and 41.24%, respectively. This result indicates that $\cdot OH$ has the most significant impact on degradation, followed by h^+, while the influence of $\cdot O_2^-$ is relatively weak. Besides, DMPO was used as the free radical scavenger to investigate HRP/Zn-CN-ZIF by EPR under visible light (>420 nm) excitation. As shown in Fig. 8b and c, compared to the dark conditions, through visible light irradiation there was a noticeable enhancement in the signals of $\cdot OH$ in the aqueous dispersion and $\cdot O_2^-$ in the methanol dispersion. The result indicates that the HRP/Zn-CN-ZIF is capable to generate $\cdot OH$ and $\cdot O_2^-$ radicals, which is also in agreement with the result of the free radical capture.

Fig. 9 reveals a potential mechanism for the photoenzyme synergistic degradation of indole by HRP/Zn-CN-ZIF according to the experimental results. After illuminated by visible light, the catalyst absorbs photons and generates hole–electron pairs. The photogenerated electrons are shifted to CB. Meanwhile, photogenerated holes migrate to the VB. Oxygen molecules dissolved in water are reduced by the photogenerated electrons on the catalyst, forming $\cdot O_2^-$ and H_2O_2. The standard redox potentials of $O_2/\cdot O_2^-$ (−0.046 eV) and O_2/H_2O_2 (0.695 eV) are lower than the CB position of HRP/Zn-CN-ZIF (−1.17 eV),[19] allowing the reduction reactions to occur. The oxidized state of HRP (HRP-Fe(III)) is reduced by photogenerated electrons. Simultaneously, the reduced state of HRP (HRP-Fe(II)) is oxidized by H_2O_2, generating $\cdot OH$ and transforming into the oxidized state (HRP-Fe(II) + H_2O_2 → HRP-Fe(III) + $\cdot OH$ + OH^-).[41] The coupling effect of the photoenzyme system continuously produces $\cdot OH$ radicals, which facilitate the degradation of indole. Noticeably, the VB position of HRP/Zn-CN-ZIF (0.67 eV) is higher than the standard redox potential of $\cdot OH/OH^-$ (2.38

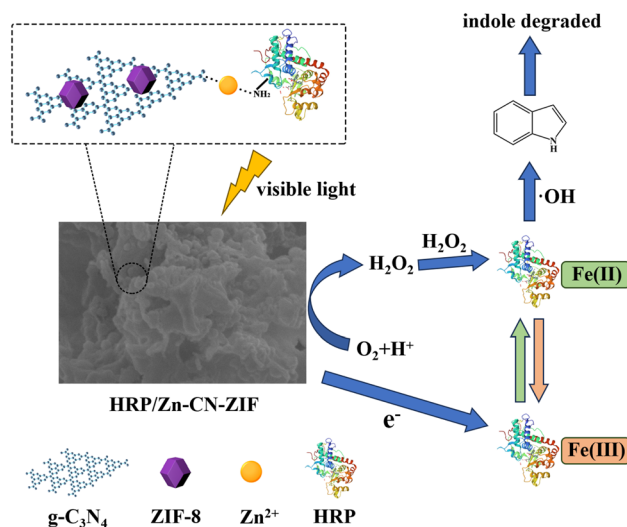Fig. 9 The possible mechanism of indole degradation by HRP/Zn-CN-ZIF.

eV).[42] Thus, it can be deduced that the generation of $\cdot OH$ is primarily caused by the reaction between HRP and H_2O_2 rather than the reaction between OH^- and photogenerated holes. Eventually, through the combined action of $\cdot OH$, $\cdot O_2^-$, and holes, indole is completely degraded.

4. Conclusions

In summary, the visible light responsive photo-peroxidase catalyst HRP/Zn-CN-ZIF was fabricated. In this reaction system, CN-ZIF was not only the carrier of the enzyme, but also served as the photocatalyst to provide free radicals and H_2O_2 for degradation. In the absence of additional H_2O_2, 20 mg L^{-1} of indole was completely degraded by HRP/Zn-CN-ZIF within 2 h under the visible light irradiation. HRP/Zn-CN-ZIF exhibited good catalytic activity at the relatively high concentration of substrate. Additionally, HRP/Zn-CN-ZIF demonstrated excellent reusability and pH stability, and also exhibited good degradation performance in different water bodies, which attributed to the stable immobilization of HRP in the photo-peroxidase catalyst. Electrochemical characterization demonstrated that
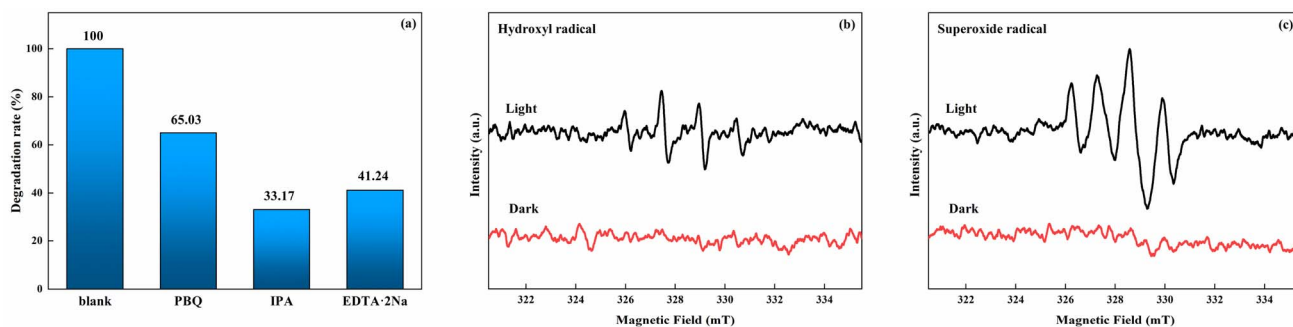

Fig. 8 Degradation of indole by HRP/Zn-CN-ZIF after adding the scavengers (a), EPR spectra of HRP/Zn-CN-ZIF for DMPO-$\cdot OH$ (b) and DMPO-$\cdot O_2^-$ (c).

HRP/Zn-CN-ZIF had excellent transfer efficiency of photo-generated charges. Free radical capture experiments and EPR measurements confirmed the critical role of ·OH in the process of redox cycle. The efficient removal of indole by HRP/Zn-CN-ZIF is mainly attributed to its excellent ability of visible light absorption and charge transfer, and the effect of photoenzyme synergistic catalysis.

Conflicts of interest

There are no conflicts to declare.

Acknowledgements

References

1 O. Botalova, J. Schwarzbauer, T. Frauenrath and L. Dsikowitzky, *Water Res.*, 2009, **43**, 3797–3812.

2 R. C. Beier, R. C. Anderson, N. A. Krueger, T. S. Edrington, T. R. Callaway and D. J. Nisbet, *J. Environ. Sci. Health, Part B*, 2009, **44**, 613–620.

3 P. K. Arora, A. Sharma and H. Bae, *J. Chem.*, 2015, **2015**, 1–13.

4 S. Ben Hammouda, N. Adhoum and L. Monser, *J. Hazard. Mater.*, 2016, **301**, 350–361.

5 M. Kaczmarek and K. Staninski, *J. Lumin.*, 2017, **183**, 470–477.

6 Q. Zhao, H. Han, S. Jia, H. Zhuang, B. Hou and F. Fang, *Desalin. Water Treat.*, 2014, **55**, 1876–1884.

7 P. Liao, S. Yuan, W. Zhang, M. Tong and K. Wang, *J. Colloid Interface Sci.*, 2012, **382**, 74–81.

8 Y. Luo, R. Zhang, G. Liu, J. Li, M. Li and C. Zhang, *J. Hazard. Mater.*, 2010, **176**, 759–764.

9 K. Fukuoka, K. Tanaka, Y. Ozeki and R. A. Kanaly, *Int. Biodeterior. Biodegrad.*, 2015, **97**, 13–24.

10 M. Bilal, H. M. N. Iqbal, H. Hu, W. Wang and X. Zhang, *Sci. Total Environ.*, 2017, **575**, 1352–1360.

11 X. Liu, P. Xue, F. Jia, K. Shi, Y. Gu, L. Ma and R. Li, *Chemosphere*, 2021, **262**, 128411.

12 O. T. Gül and I. Ocsoy, *Mater. Lett.*, 2021, **303**, 130501.

13 M. Bilal, T. Rasheed, H. M. N. Iqbal, H. Hu, W. Wang and X. Zhang, *Int. J. Biol. Macromol.*, 2018, **113**, 983–990.

14 F. X. Ye, R. F. Zhu and Y. Li, *J. Hazard. Mater.*, 2009, **167**, 148–153.

15 H. Zhang, J. Wu, J. Han, L. Wang, W. Zhang, H. Dong, C. Li and Y. Wang, *Chem. Eng. J.*, 2020, **385**, 123764.

16 H. Dong, N. Song, M. Yan, H. Wu, H. Zhang, C. Ma and Y. Wang, *Chin. Chem. Lett.*, 2021, **32**, 2047–2051.

17 L. Jiang, L. Lin, D. Chen, Y. Wang, M. Li, M. Shi, Y. Tang and Y. Qiu, *Mater. Chem. Phys.*, 2020, **243**, 122643.

18 B. Chen, Y. Wang, S. Shen, W. Zhong, H. Lu and Y. Pan, *Small Methods*, 2024, 2301598.

19 C. Li, S. Yu, L. Gu, J. Han, H. Dong, Y. Wang and G. Chen, *Adv. Mater. Interfaces*, 2018, **5**, 1801297.

20 T. Zhou, H. Wei, B. Xiao, T. Lv, L. Duan, Q. Lu, J. Zhang, Y. Zhang and Q. Liu, *RSC Adv.*, 2023, **13**, 8915–8922.

21 P. Xiong, Q. Li, Q. Tang, H. Wang and Z. Wu, *RSC Adv.*, 2023, **13**, 31820–31834.

22 J. Hu, P. Zhang, W. An, L. Liu, Y. Liang and W. Cui, *Appl. Catal., B*, 2019, **245**, 130–142.

23 C. Li, Y. Xu, W. Tu, G. Chen and R. Xu, *Green Chem.*, 2017, **19**, 882–899.

24 E. Bilgin Simsek and D. Saloglu, *J. Mol. Liq.*, 2021, **337**, 116612.

25 Y. Shiraishi, S. Kanazawa, Y. Kofuji, H. Sakamoto, S. Ichikawa, S. Tanaka and T. Hirai, *Angew. Chem., Int. Ed.*, 2014, **53**, 13454–13459.

26 Y. Zhao, Y. Liu, J. Cao, H. Wang, M. Shao, H. Huang, Y. Liu and Z. Kang, *Appl. Catal., B*, 2020, **278**, 119289.

27 F. Zhang, B. Zheng, J. Zhang, X. Huang, H. Liu, S. Guo and J. Zhang, *J. Phys. Chem. C*, 2010, **114**, 8469–8473.

28 M. M. Bradford, *Anal. Biochem.*, 1976, **72**, 248–254.

29 F. Dong, L. Wu, Y. Sun, M. Fu, Z. Wu and S. C. Lee, *J. Phys. Chem. C*, 2011, **21**, 15171.

30 M. Zhang, Q. Shang, Y. Wan, Q. Cheng, G. Liao and Z. Pan, *Appl. Catal., B*, 2019, **241**, 149–158.

31 X. Liu, J. Zhang, Y. Dong, H. Li, Y. Xia and H. Wang, *New J. Chem.*, 2018, **42**, 1218–12187.

32 R. Muruganantham, F. Wang, R. A. Yuwono, M. Sabugaa and W. Liu, *Energy Fuels*, 2021, **35**, 10878–10889.

33 Y. Liu, G. Xu, D. Ma, Z. Li, Z. Yan, A. Xu, W. Zhong and B. Fang, *J. Cleaner Prod.*, 2021, **328**, 129745.

34 Y. Liu, S. Shen, Z. Li, D. Ma, G. Xu and B. Fang, *Mater. Charact.*, 2021, **174**, 111031.

35 H. S. Moon, K. C. Hsiao, M. C. Wu, Y. Yun, Y. J. Hsu and K. Yong, *Adv. Mater.*, 2023, **35**, 2200172.

36 C. Li, G. Chen, J. Sun, Y. Feng, J. Liu and H. Dong, *Appl. Catal., B*, 2015, **163**, 415–423.

37 H. Liu, D. Cheng, F. Chen and X. Zhan, *Catal. Sci. Technol.*, 2020, **10**, 351–359.

38 H. Che, G. Che, E. Jiang, C. Liu, H. Dong and C. Li, *J. Taiwan Inst. Chem. Eng.*, 2018, **91**, 224–234.

39 Y. Liu, W. Yin, Q. Lin, Z. Li, W. Zhong and B. Fang, *Appl. Surf. Sci.*, 2023, **640**, 158386.

40 F. K. de Oliveira, L. O. Santos and J. G. Buffon, *Food Res. Int.*, 2021, **143**, 110266.

41 J. L. Olloqui-Sariego, G. S. Zakharova, A. A. Poloznikov, J. J. Calvente, D. M. Hushpulian, L. Gorton and R. Andreu, *ACS Catal.*, 2016, **6**, 7452–7457.

42 J. Xia, M. Ji, J. Di, B. Wang, S. Yin, Q. Zhang, M. He and H. Li, *Appl. Catal., B*, 2016, **191**, 235–245.